LATTICE–BOLTZMANN SIMULATIONS IN COMPUTATIONAL HEMODYNAMICS

Daniel R. Golbert
Pablo J. Blanco
Raúl A. Feijóo
danielrg@lncc.br
pjblanco@lncc.br
feij@lncc.br
Laboratório Nacional de Computação Científica, Av. Getúlio Vargas 333, Quitandinha, 25651–075, Petrópolis, RJ, Brasil
Instituto Nacional de Ciência e Tecnologia em Medicina Assistida por Computação Científica, Av. Getúlio Vargas 333, Quitandinha, 25651–075, Petrópolis, RJ, Brasil

Abstract. *Recently, the interest in Lattice–Boltzmann models by the computational fluid dynamics community has notoriously increased with the purpose of modeling complex flows. For instance, computational hemodynamics has been an area of research where this kind of methodologies have received significant attention during last years. In this work, we implement a Lattice–Boltzmann model with the aim of simulating blood flows in the major arteries. The selected model, based on a single-relaxation-time approach, is briefly described in combination with second order boundary conditions for both velocity and pressure and proper equilibrium distributions that take care of the incompressible behavior of the fluid. After the description of the model several numerical examples are presented. In 2D and 3D we employ the Womersley and Driven Cavity problems as benchmarks. As well, the simulation of blood flows in an arterial bend and in an aneurismal region, both artificially created, are performed. The numerical results are assessed within a framework in which the values of the parameters that set up the physical regimes in the simulations are suitably tuned in order to guarantee the accuracy.*

Keywords: *Lattice–Boltzmann, Incompressible flow, Hemodynamics*

1. INTRODUCTION

Since its introduction in the 80's the Lattice–Boltzmann Method (LBM) has been through several refinements and extensions and became a promising numerical scheme for simulating the complex fluid dynamics in the most varied applications. In particular, LBM has been employed systematically during the last few years in a series of computational hemodynamics applications. For example, in the simulation of blood flows in mechanical heart valves (Pelliccioni et al., 2007), in aneurisms (Hirabayashi et al., 2006), in the abdominal aorta (Artoli et al., 2006), among others.

Differing from the conventional methods based on the discretization of continuum macroscopic equations, LBM is a mesoscopic particle based method derived from the Lattice-Gas Cellular Automata method (Rothman and Zaleski, 2004) and the Boltzmann Equation (Abe, 1997). Its basic idea is to build a simplified kinetic model that incorporates the essential physics of microscopic processes, such that the macroscopic system properties obey the imposed equations.

In this work we will introduce, in Section 2, the governing equations of LBM with BGK approximation (referring to the work of Bhatnagar et al. (1954)) and the chosen methods for implementing boundary conditions. In Section 3 will be presented an analysis of the parameters used in the simulations of fluid flows and how to tune them for obtaining better results. And in Section 4 we will show results obtained from the implementations of the method in some benchmark problems, in 2D and 3D, and in two computational hemodynamics problems. Finally, we discuss some conclusions and prospects in Section 5.

2. METHODS

The Lattice–Boltzmann Method with BGK approximation is a Lagrangian and explicit method. It is based on the movement and collision of micro-particles distributions, described by the equation:

$$f_i(\vec{x} + \Delta x\vec{e_i}, t + \Delta t) - f_i(\vec{x}, t) = \frac{1}{\tau}\left[f_i^{\text{eq}}(\vec{x}, t) - f_i(\vec{x}, t)\right], \; i = 0, \ldots, \ell, \tag{1}$$

where, $f_i(\vec{x}, t)$ represents the micro-particles distribution density at position $\vec{x}$ and time t, moving towards the direction $\vec{e_i}$ of the lattice, Δx is the lattice spacing, Δt is the time step and ℓ is the number movement directions of the lattice. The relaxation parameter τ is related to the kinematic viscosity of the fluid as

$$\nu = (2\tau - 1)\Delta x^2/6\Delta t. \tag{2}$$

The chosen equilibrium distribution (He and Luo, 1997) was design to reduce the implicit compressibility of the method

$$f_i^{\text{eq}} = \omega_i \left\{\rho + \rho_0\left[3\frac{(v\vec{e_i}\cdot\vec{u})}{v^2} + \frac{9}{2}\frac{(v\vec{e_i}\cdot\vec{u})^2}{v^4} - \frac{3}{2}\frac{(\vec{u}\cdot\vec{u})}{v^2}\right]\right\}, \; i = 0, \ldots, \ell, \tag{3}$$

where, $v = \Delta x/\Delta t$ is the particles speed, the weights ω_i are lattice model dependent, ρ_0 is the average density (constant), ρ and u are the density and velocity of the fluid, calculated from the mass and momentum conservation equations:

$$\rho(\vec{x}, t) = \sum_{i=0}^{\ell} f_i(\vec{x}, t) \quad \text{and} \quad \rho_0\vec{u}(\vec{x}, t) = \sum_{i=1}^{\ell} v\vec{e_i} f_i(\vec{x}, t). \tag{4}$$

In this model, the normalized pressure is calculated as function of the density: $P = c_s^2 \rho / \rho_0$, where $c_s = v/\sqrt{3}$ is the speed of sound.

In Fig. 1 are shown the allowed movement movement directions for the two-dimensional lattice model $D2Q9$ (left) and for the three-dimensional lattice model $D3Q19$ (right) (see A.M. Artoli (2006)), both implemented in this work. These models allow the particles to stand still or to move in other 8 directions ($D2Q9$) or 18 directions ($D3Q19$).

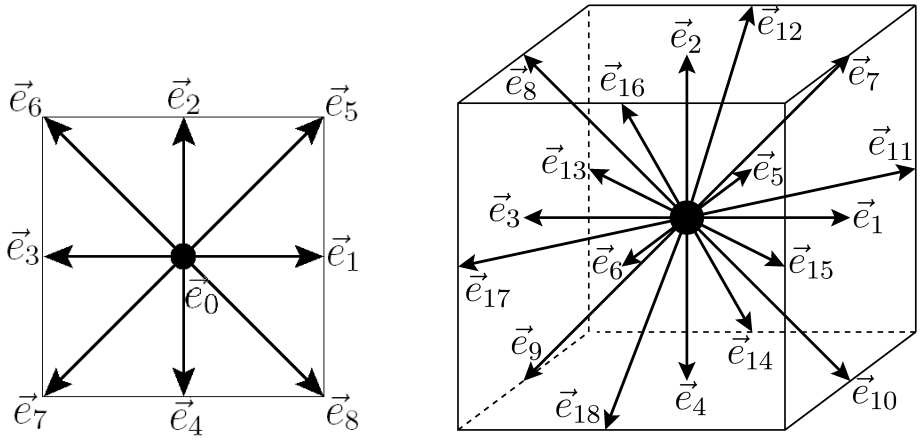

Figure 1: Allowed movement movement directions for the two-dimensional lattice model $D2Q9$ (left) and for the three-dimensional lattice model $D3Q19$ (right).

The mentioned weights for the equilibrium distribution equation (Eq. (3)) for the lattice model $D2Q9$ are: $\omega_0 = 4/9,\ \omega_{1-4} = 1/9,\ \omega_{5-8} = 1/36$. And, for the model $D3Q19$ are: $\omega_0 = 1/9,\ \omega_{1-6} = 1/18,\ \omega_{7-18} = 1/36$.

To impose the pressure boundary conditions, we adopted the model propose by Zou and He (1997), designed for flat surfaces. This model make use of the conservation equations (Eq. (4)) and the reflection of some symmetric non-equilibrium distributions ($f_i^{\text{neq}} = f_i - f_i^{\text{eq}}$) to impose the desired pressure. And we chose an interpolation model (Guo et al., 2002) to impose the velocity boundary conditions on curved surfaces. The use of an interpolation model is interesting for imposing the boundary conditions on surfaces that do not cross the lattice points exactly, for instance, like the curved walls of an artery.

3. PARAMETERS TUNING

When choosing the parameters for a simulation via LBM, one has to do a balance between computational cost and precision. In order to achieve the expected results, one has to choose (calculate) the parameters accordingly and, after that, modify (tune) them, if necessary.

The main parameter of the method τ is specially responsible for the numerical stability, its minimum acceptable value is simulation dependent, but we obtained stable simulations with $\tau > 0.52$. Keep in mind that this parameter becomes smaller as ν and Δt get smaller and as Δx gets bigger (lattice refinement), so a lattice refinement is usually the key to increase τ.

It is also important to keep the Mach number, described as $M = u_{max}/c_s$, at a small value, usually less than 0.15. So that the distributions of micro-particles induce the macro behavior of an incompressible fluid. And also, the lattice has to be enough refined in order to capture de velocity gradients of the fluid.

And, for transient simulations, the characteristic oscillation period (T) should be much smaller than the propagation time (L/c_s) of information over the characteristic length (L) of the problem, so that no spurious compressibility effect takes place. In the presented implementations, we adopted T at least 30 times greater than L/c_s.

An analysis of the effect, on the parameters, of three tactics to tune a transient simulation is presented in Tab. 1. The three tactics are to increase the number of time steps per cycle, to refine the lattice or do both. In this table, the symbol ' indicates how much the parameter changes, $\tau_r = \tau - 0.5$, "cost" represents the computational cost of a simulation cycle and $(\cdot)$ indicates the 3D case (shown only when the number differs from the 2D case).

Table 1: Tactics to tune a transient simulation and how they have effect on the parameters and on the cost of each cycle.

Tactic	steps'	Δt'	lattice points'	Δx'	$T/(L/c_s)$'	τ_r'	Mach'	cost'
Increase steps	n	$1/n$	1	1	n	$1/n$	$1/n$	n (n)
Refine lattice	1	1	n^2 (n^3)	$1/n$	$1/n$	n^2	n	n^2 (n^3)
Do both	n	$1/n$	n^2 (n^3)	$1/n$	1	n	1	n^3 (n^4)

This table shows that increasing the number of steps per cycles solo has a small cost increase, but may lead to undesired results, like the decrease of τ and of the relation $T/(L/c_s)$. Which can be reverted by refining the lattice, at a greater computational cost.

4. RESULTS

This section is divided in two parts, first we will present some benchmark problems for validation and analysis purposes and in the second part some results from the implementation of computational hemodynamics problems will be discussed.

4.1 Benchmarks

There will be presented four benchmark problems for the verification and analysis of the chosen model for implementation. The stationary Driven Cavity problem and the transient Womersley flow problem will be tested in 2D and 3D.

Driven Cavity in 2D. The Driven Cavity problem is widely used for testing numerical simulations of incompressible fluid flows, with the objective of testing the accuracy and convergence of numerical methods. This problems consists of a square cavity with impermeable non-slip walls, such that only the upper wall moves with constant velocity (of module U_{max}) to the right (direction $\vec{x}$). Therefore, the flow in induced by the diffusion of viscous effects coming from the wall movement.

This problem is characterized by the adimensional Reynolds number, here calculated as

$$Re = \frac{LU_{max}}{\nu}, \tag{5}$$

where, L is the walls length and ν is the kinematic viscosity (see Eq. (2)).

In Fig. 2 we present some results of simulations with Reynolds number equal to 1000 and three lattices with 64×64, 128×128 and 256×256 points. On the left side, are plotted the velocity components u_x (horizontal) and u_y (vertical) along the vertical and horizontal lines that cross the center, respectively, extracted from simulations of the present implementation (where "LBabc" means a simulation with lattice size $abc \times abc$) and from the well known reference Ghia et al. (1982), as the problem has no analytical solution. One can see from this figure that our results approach the ones from the reference consistently as the lattice is refined. And on the right side, there are plotted some streamlines, where one can identify the vortices and visualize the stationary flow structure, extracted from a simulation via LBM with lattice size 256×256.

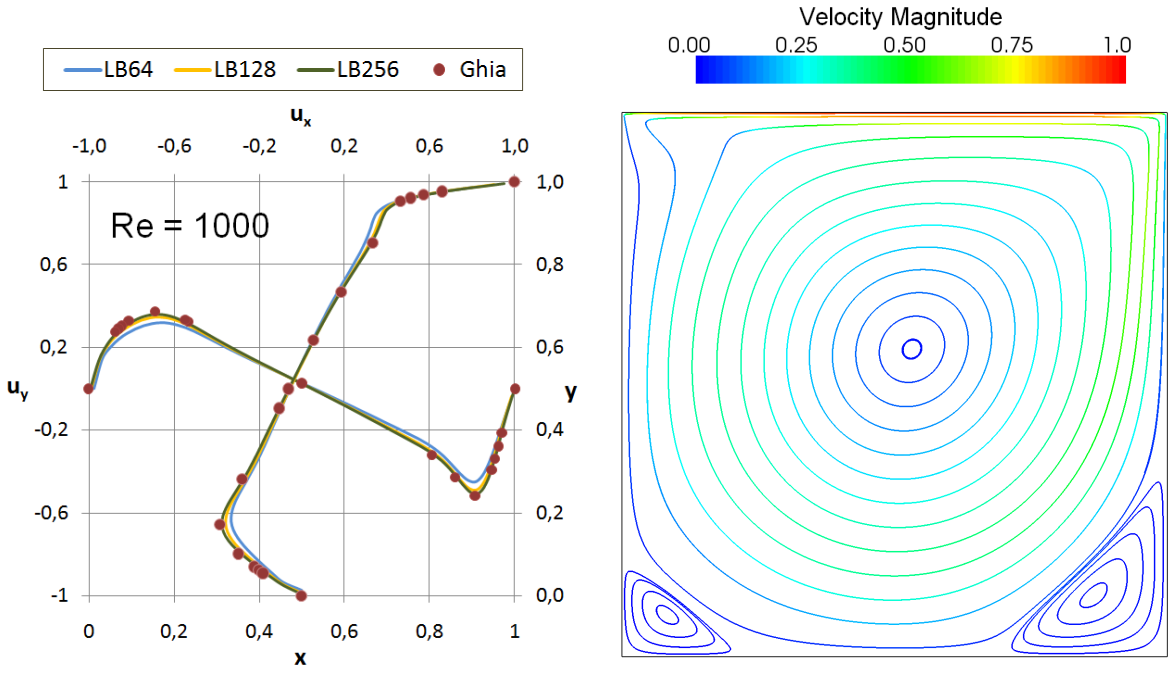

Figure 2: Results of simulations with Reynolds number 1000. On the left, velocity components u_x and u_y are plotted over the vertical and horizontal lines that cross the center, respectively, obtained from simulations via LBM, with different lattice sizes, and from Ghia et al. (1982). On the right, some streamlines and vortices from a simulation via LBM are shown.

From the streamlines shown in Fig. 2 we have determined the three vortices centers and compared them with data from literature, as presented in Tab. 2. Here, one can see that the positions are in good agreement with the literature.

Table 2: Main vortices position extracted from the results of a simulation via LBM in a lattice with 256×256 points (LB256) and from the indicated references, with Reynolds number 1000.

Vortex	Central		Left		Right	
Reference	x	y	x	y	x	y
LB256	0,532	0,565	0,0831	0,0771	0,865	0,112
Ozawa (1975)	0,533	0,569				
Ghia (1982)	0,5313	0,5626	0,0859	0,0785	0,8594	0,1094

The main points to check while implementing a stationary problem via LBM are its main parameter τ (for numerical stability), the Mach number (U_{max}/c_s), which was kept at 0.17 for this problem, and the lattice refinement (for better capturing the details of the velocity field).

Womersley flow in 2D. The Womersley flow is an intrinsically transient problem with analytical solution to the Navier-Stokes equations (Fang et al., 2002). It consists of a fluid confined in a channel with constant pressure on the right side (p_{out}) and with an oscillatory pressure on the left side (p_{in}), like the function bellow:

$$\Delta p(t) = \frac{p_{out} - p_{in}(t)}{L_x} = -A\cos(\mu t) \tag{6}$$

where, $\Delta p(t)$ is the pressure gradient at time t, A is its amplitude, L_x is the channel length, $\mu = 2\pi/T$ is the angular frequency and T is the boundary condition oscillation period.

This problem is characterized by the adimensional Womersley number (κ), calculated here as:

$$\kappa = \frac{L_y}{2}\sqrt{\frac{\mu}{\nu}}, \tag{7}$$

where, L_y is the channel width.

The simulations for this case were done with a fixed Reynolds number of 30 and in a channel with aspect ratio ($L_x \times L_y$) equal to 2×1. The tested Womersley numbers ranged from 3.5 to 15 and the lattice sizes from 64×32 to 256×128. In Fig. 3 are plotted the velocity profile along a period extracted from simulations via LBM (in dashed black lines) with a lattice size of 64×32 and a Womersley number of 3.5 (left) and with a lattice size of 256×128 and a Womersley number of 15 (right), together with the corresponding analytical solutions (in colored lines). From these results and from the fact that the flux difference between inlet and outlet of the channel in the simulations was less than 2%, we conclude that the chosen lattices and parameters were tuned so that the phenomenology of the problem was accurately reproduced.

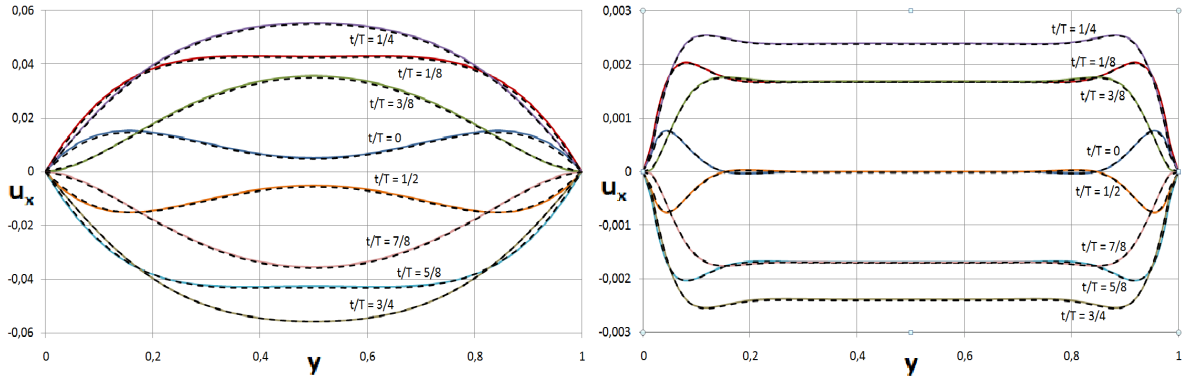

Figure 3: Velocity profiles along a period of simulations with Womersley 3.5 (left) and 15 (right) in lattices of size 64×32 and 256×128, respectively, via LBM (in dashed black lines) and the corresponding analytical solutions (in colored lines).

The main point to check while implementing a transient problem via LBM, besides the ones mentioned for the stationary case, is the relation $T/(L/c_s)$ that has to be high in order to minimize the inlet and outlet flux difference (spurious compressibility effects). A better study of this relation will be presented for the three-dimensional case of the Womersley flow.

Driven Cavity in 3D. This problem is similar to the 2D case, but now the fluid is confined in a cubic cavity with the upper wall moving in the $\vec{x}$ (horizontal) direction at speed U_{max}. Again, this problem is characterized by the Reynolds number (see Eq. (5)).

For this problem, we have simulated cases with a Reynolds number range from 100 until 1000. In Fig. 4 we present some results of simulations with Reynolds number 100 (top subfigures) and 1000 (bottom subfigures). As this problem has no analytical solution, we compared, on the left side of the figure, results obtained from the present implementation with results from the work of Yang et al. (1998). More specifically, we compared the velocity components u_x (horizontal) and u_y (vertical) over lines on the $\vec{y}$ and $\vec{x}$ directions that cross the center, respectively, obtained from the mentioned reference and from simulations via LBM with lattice sizes

$50 \times 50 \times 50$, $100 \times 100 \times 100$ and $200 \times 200 \times 200$. This figure shows that for the problem with Reynolds number 100 the results obtained via LBM are close to the ones obtained in the reference with a less refined lattice (with $50 \times 50 \times 50$ points) and for the problem with Reynolds number 1000 the results obtained via LBM get closer to the reference results as the lattice is refined. On the right side of this figure are plotted some velocity isosurfaces that show the tridimensional structure of the velocity field. Here, we also notice the displacement of the main vortex and the appearing of a new vortex as the Reynolds number changes.

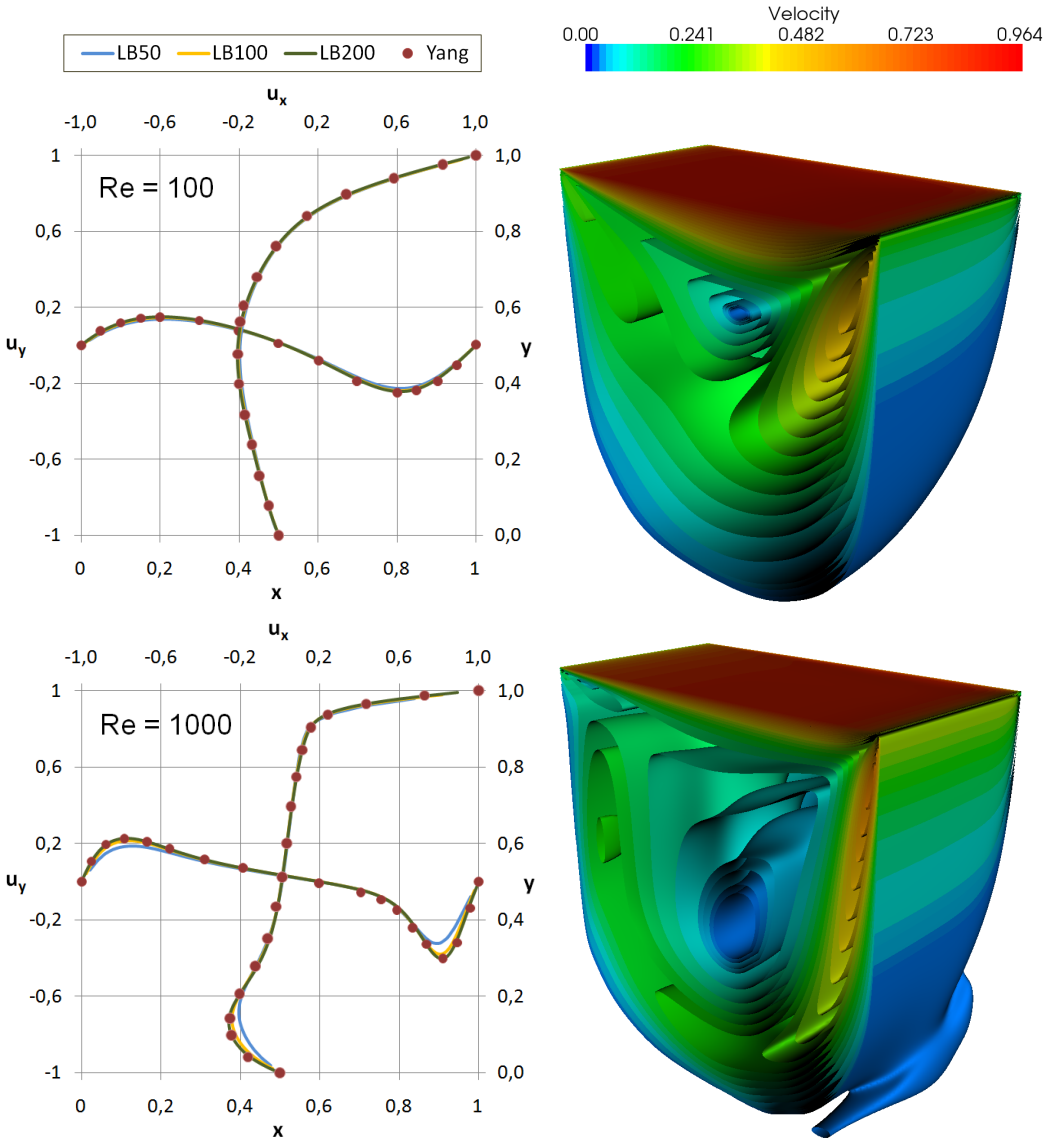

Figure 4: On the left are compared the velocity components u_x (horizontal) and u_y (vertical) over lines on the $\vec{y}$ and $\vec{x}$ directions that cross the center, respectively, obtained from Yang et al. (1998) and from simulations via LBM with different lattice sizes. On the right are some velocity isosurfaces that show the tridimensional structure of the velocity field.

Womersley flow in 3D. Like in the 2D case, this problem has analytical solution (A.M. Artoli, 2006) and consists of an incompressible fluid confined in a cylindrical tube with constant

pressure on the right extremity (p_{out}) and an oscillatory pressure on the left extremity (p_{in}), like:

$$\Delta p(t) = \frac{p_{out} - p_{in}(t)}{L_x} = -A\cos(\mu t). \tag{8}$$

The problem is again characterized by the Womersley number, calculated as:

$$\kappa = R\sqrt{\frac{\mu}{\nu}}, \tag{9}$$

where, R is the tube radius.

We simulated this problem with a fixed Reynolds number of 1, and with Womersley numbers ranging from 3.5 to 20. In order to obtain results close to the analytical solutions we employed the tactics presented on Section 3.

This problem was used to analyze how the aspect ratio (length×width) and the relation $T/(L/c_s)$ have effect on the compressibility error (flux difference between outlet and inlet). This study was done by simulating problems with a fixed Womersley number of 3.5 and aspect ratios ranging from 2×1 to 16×1. We started the simulations with 1312 time steps per cycle and double this quantity until the compressibility error got close to 1%. In Tab. 3 are shown the compressibility error and the relation $T/(L/c_s)$ (referred as T_r) for the simulated cases, where "*" indicates unstable and "–" indicates not simulated. From this table one can see that there is a direct relation between the relation T_r and the compressibility error, indicating that $T_r \geq 48$ should lead to small compressibility errors.

Table 3: Compressibility errors of simulations with different aspect ratios.

$N_t/1312$	1		2		4		8		16		32	
A.R.	error	T_r	error	T_r	error	T_r	error	T_r	error	T_r	error	T_r
1×1	2.91%	24	0.70%	48	–	–	–	–	–	–	–	–
2×1	16.7%	12	3.67%	24	0.88%	48	–	–	–	–	–	–
4×1	166%	6	18.5%	12	4.00%	24	0.97%	48	–	–	–	–
8×1	*	3	168%	6	19.1%	12	4.16%	24	1.00%	48	–	–
16×1	*	1.5	*	3	167%	6	19.4%	12	4.13%	24	1.06%	48

In Fig. 5 one can see that the velocity profiles do not change along the tube if we set the relation $T_r = 48$, even with at aspect ratio of 16×1.

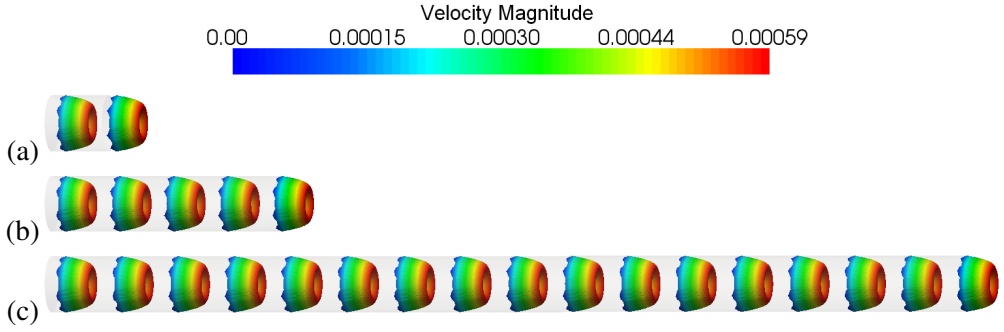

Figure 5: Velocity profiles along the tube at the time $t = 0$ obtained from simulations with Womersley number 3.5 in tubes with aspect ratios of: (a) 1×1,(b) 4×1 and (c) 16×1.

We also compared the results of simulations via LBM with Womersley numbers 3.5 (left) and 20 (right) with lattices of size $64 \times 32 \times 32$ and $256 \times 128 \times 128$, respectively, in a tube with aspect ratio 2×1 against the analytical solutions in Fig. 6. In this figure are plotted 8 velocity profiles, over a transversal line that crosses the center of the tube, along a cycle obtained from simulations via LBM (in dashed black lines) and from the analytical solutions (in colored lines). The good agreement between the solutions was reached by using the tactics presented in Section 3.

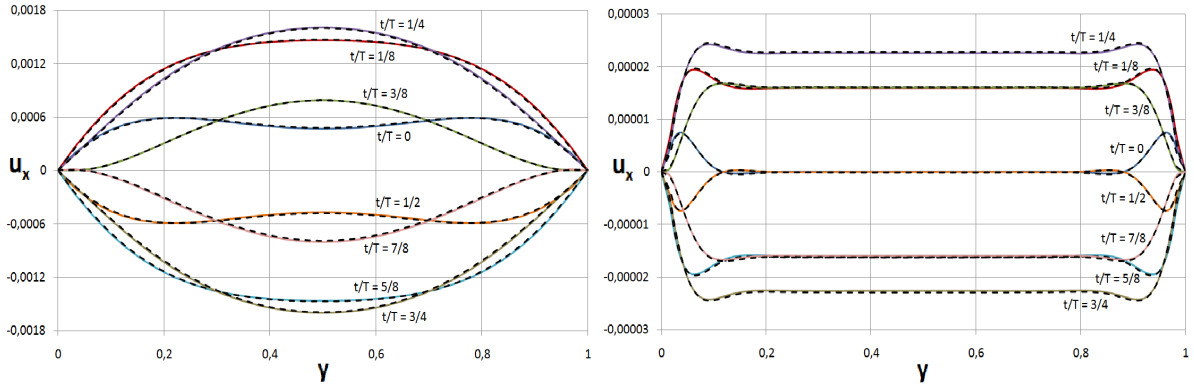

Figure 6: Velocity profiles, over a transversal line, along a cycle obtained from simulations via LBM (in dashed black lines) and from the analytical solutions (in colored lines) of problems with Womersley numbers 3.5 (left) and 20 (right) in a tube with aspect ratio 2×1.

4.2 Problems in hemodynamics

Here we present the method's capability of simulating problems with physical properties that are common in computational hemodynamics. In the next two problems we will model the blood flow, in an arterial bend and in an artery with an aneurism, as a Newtonian incompressible fluid with kinematic viscosity equal to $0.035\text{cm}^2/\text{s}$.

Arterial bend. In this problem we wish to model the blood flow in a cylindrical arterial bend with aspect ratio 18×1 driven by a pulsatile inflow at the superior extremity. The geometry of the artery is described in Fig. 7.

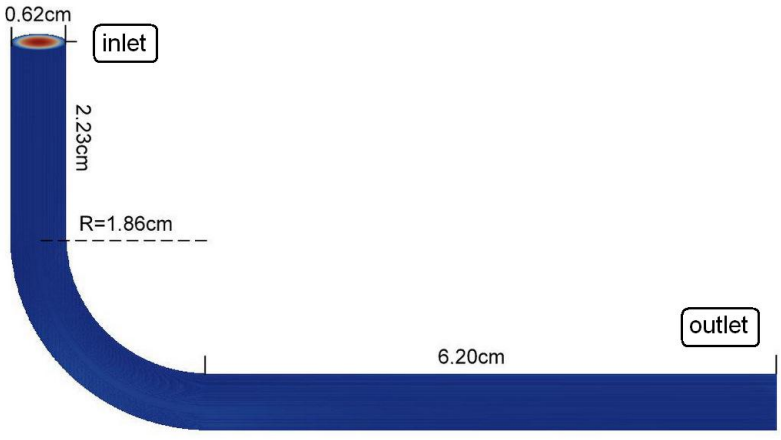

Figure 7: Arterial bend geometry description.

The pulsatile inflow is assumed to have a parabolic profile and has an average speed described by:

$$\overline{u}_{in}(t) = U\left[1 - \cos\left(\frac{2\pi t}{T}\right)\right], \tag{10}$$

where, $T = 0.75$s represents the pulse period and $U = 16.9$cm/s is the average speed of the fluid at the inlet along a period. On the other extremity of the geometry is imposed a constant reference pressure.

From the above parameters we conclude that this problem is characterized by a Womersley number of 4.8 and a Reynolds number of 900.

In Fig. 8 are plotted some velocity profiles (left) and a representation of the secondary flow that takes place (right) on a simulation with approximately 90 points over the artery diameter, when the fluid reaches its top speed. On the left subfigure, we can see how the method captured the velocity profile deformation along the bend and its reconstruction at the end, because of the high aspect ratio. This profile deformation occurs specially because of the 90 degrees curvature and the high Reynolds number. And on the right subfigure, the transversal slices along the artery put in evidence the secondary vortices structures, showing the complexity of the flow.

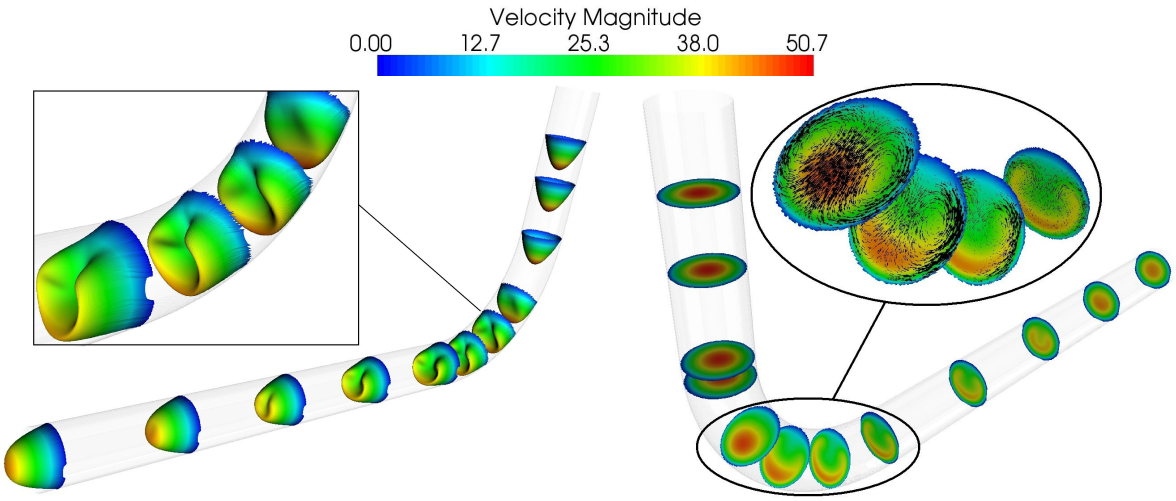

Figure 8: Velocity profiles (left) and the secondary flow that takes place (right) when the fluid reaches its top speed.

The high aspect ratio of the problem led us to adopt a very refined lattice in order to keep the relation $T/(L/c_s)$ above 30 and, with that, we obtained a compressibility error of less than 2%.

Artery with an aneurism. In this problem we wish to see how the blood behaves in an aneurism. For that we modeled the blood flow in a cylindrical artery, with aspect ratio 10×1, that has a spherical aneurism driven by a pulsatile pressure on the left extremity. The geometry of the artery is described in Fig. 9.

The oscillatory pressure at the inlet in described by:

$$p_{in}(t) = p_{out} + C(\cos(\mu t) + 1), \tag{11}$$

where, the constants C and μ were chosen such that problem is characterized by a Womersley number of 4.5 and a Reynolds number of 400.

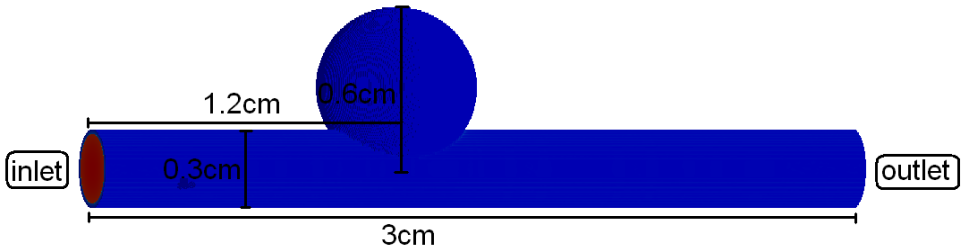

Figure 9: Geometry description of the artery with an aneurism.

In Fig. 10 are plotted some velocity isosurfaces (left) and a representation of the secondary flow over some slices (right), when the fluid reaches its minor (top) and major (bottom) speeds. The left subfigures indicate the structure of the flow in the region of the aneurism and show the main vortex displacement. The subfigures on the right shows how the secondary flow changes, specially inside the aneurism, in two instants of the pulse. In this simulation we used the relation $T/(L/c_s)$ equal to 30 which led to a less then 1% compressibility error.

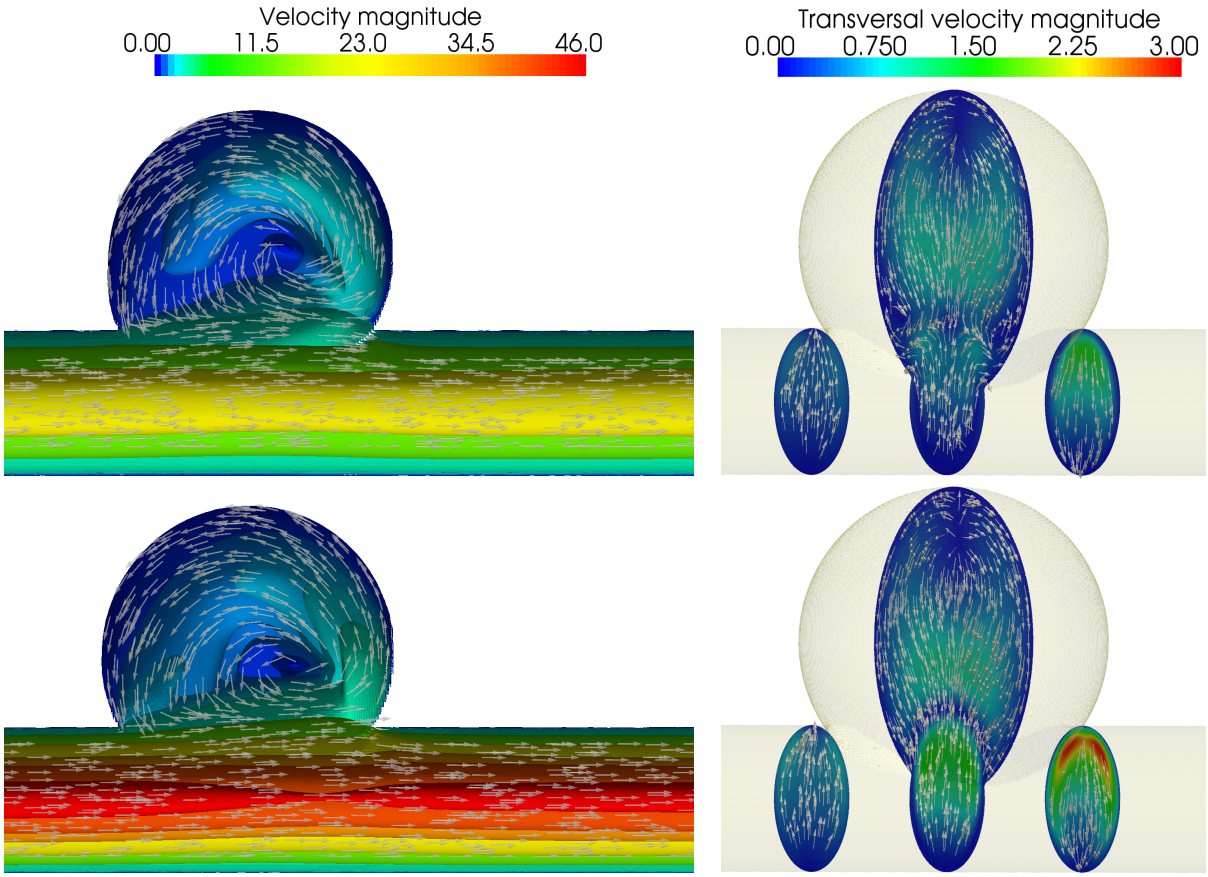

Figure 10: Some velocity isosurfaces (left) and a representation of the secondary flow over some transversal slices (right), when the fluid reaches its minor (top) and major (bottom) speeds.

5. CONCLUSIONS

With the analysis of the implemented cases we conclude that the Lattice–Boltzmann Method, together with the chosen equilibrium distribution and the models for implementing the boundary conditions, was capable of simulating the phenomenology of the problems. More specifically, we have successfully implemented problems in two and three dimensions, that were station-

ary and transient, with Reynolds numbers ranging from 1 to 1000, with Womersley numbers ranging from 3.5 to 20 and aspect ratios ranging from 1×1 to 18×1.

An essencial part of the mentioned implementations was to correctly tune the involved parameters as explained in Section 3 and experimented in Section 4. The four main parameters to keep in mind are the relaxation parameter τ, the Mach number, the relation $T/(L/c_s)$ and the lattice refinement.

As a continuation of this work we will extract more results from the analysis of the hemodynamic problems, like the study of the walls tensions or the remain time of the blood inside the aneurism. Also we are working on the simulation of blood flow in geometries obtained from patient specific medical images.

REFERENCES

Abe, T., 1997. Derivation of the lattice boltzmann method by means of the discrete ordinate method for the boltzmann equation. *J. Comp. Phys.*, vol. 131, pp. 241–246.

A.M. Artoli, A.G. Hoekstra, P. S., 2006. Optimizing lattice boltzmann simulations for unsteady flows. *Computers & Fluids*, vol. 35, pp. 227–240.

Artoli, A., Hoekstra, A., & Sloot, P., 2006. Mesoscopic simulations of systolic flow in the human abdominal aorta. *Journal of Biomechanics*, vol. 39, n. 5, pp. 873–884.

Bhatnagar, P., Gross, E., & Krook, M., 1954. A model for collision processes in gases: small amplitude processes in charged and neutral one-component system. *Phys. Rev.*, vol. 94, pp. 511–525.

Fang, H.-P., Wan, R.-Z., & Lin, Z.-F., 2002. Lattice boltzmann model with nearly constant density. *Physical Review E*, vol. 66, n. 3, pp. 036314.

Ghia, U., Ghia, K. N., & Shin, C. T., 1982. High-re solutions for incompressible flow using the navier-stokes equations and a multigrid method. *Journal of Computational Physics*, vol. 48, pp. 387–411.

Guo, Zheng, & Shi, 2002. An extrapolation method for boundary conditions in lattice boltzmann method. *Phys. Fluids*, vol. 14, n. 6, pp. 2007–2010.

He, X. & Luo, L., 1997. Lattice boltzmann model for the incompressible navier–stokes equation. *J. Stat. Phys.*, vol. 88, pp. 927–944.

Hirabayashi, M., Ohta, M., Baráth, K., Rüfenacht, D., & Chopard, B., 2006. Numerical analysis of the flow pattern in stented aneurysms and its relation to velocity reduction and stent efficiency. *Math. Comput. Simul.*, vol. 72, n. 2-6, pp. 128–133.

Pelliccioni, O., Cerrolaza, M., & Herrera, M., 2007. Lattice boltzmann dynamic simulation of a mechanical heart valve device. *Math. Comput. Simul.*, vol. 75, n. 1-2, pp. 1–14.

Rothman, D. H. & Zaleski, S., 2004. *Lattice-gas cellular automata: simple models of complex hydrodynamics*. Cambridge University Press.

Yang, J.-Y., Yang, S.-C., Chen, Y.-N., & Hsu, C.-A., 1998. Implicit weighted eno schemes for the three-dimensional incompressible navier-stokes equations. *J. Comput. Phys.*, vol. 146, n. 1, pp. 464–487.

Zou, Q. & He, X., 1997. On pressure and velocity boundary conditions for the lattice boltzmann bgk model. *American Institute of Physics*, vol. 9, n. 6, pp. 1591–1598.